Tannic acid post-treatment of enzymatically crosslinked chitosan-alginate hydrogels for biomedical applications

[a]Hafez Jafari*, [a]Pejman Ghaffari-bohlouli, [b]Daria Podstawczyk, [c]Lei Nie, [a]Amin Shavandi*

[a]Université libre de Bruxelles (ULB), École polytechnique de Bruxelles, 3BIO-BioMatter, Avenue F.D. Roosevelt, 50 - CP 165/61, 1050 Brussels, Belgium

[b]Department of Process Engineering and Technology of Polymer and Carbon Materials, Faculty of Chemistry, Wroclaw University of Science and Technology, Norwida 4/6, Wroclaw, 50–373 Poland

[c]College of Life Sciences, Xinyang Normal University (XYNU), Xinyang 464000, China

* Corresponding authors: Email: Seyed.Hafez.Jafari@ulb.be, amin.shavandi@ulb.be , Tel: +326503681

Abstract

Enzyme-mediated crosslinked hydrogels as soft materials for biomedical applications have gained considerable attention. In this article, we studied the effect of post-treatment with tannic acid on adhesiveness and physiochemical properties of an enzymatically crosslinked hydrogel based on chitosan and alginate. The hydrogels were soaked in TA solution at different pH (3, 5.5, 7.4, and 9) and concentrations (1, 10, 20, 30 TA wt%). Increasing the TA concentration to 30 TA wt% and pH (up to 7.4) increased the TA loading and TA release. TA post-treatment reduced the swelling ratio and degradation rate of the hydrogels due to the formation of hydrogen bonding between TA molecules, chitosan, and alginate chains due to the increasing the secondary crosslinking density. TA-reinforced hydrogels with 30% TA (Gel-TA 30) exhibited significantly high adhesive strength (up to 18 kPa), storage modulus (40 kPa), and antioxidant activity (>96%), antibacterial activity, and proliferation and viability of 3T3-L1 fibroblast cells.

Keywords: Marine polysaccharides; Adhesive hydrogels; Tannic acid treatment; Enzymatic crosslinking

1. Introduction

The development of adhesive hydrogels has attracted much scientific consideration in clinical applications such as wound closure, tissue sealants, and hemostatic and wearable biosensors (Z. Chen et al., 2021; Xiao Hu, Xia, Huang, & Qian, 2019; Suneetha, Rao, & Han, 2019). However, the design of adhesive biomaterials with adequate adhesiveness and biocompatibility is highly challenging (Le et al., 2018; Xie et al., 2015). Adhesion is defined as cohesion to withstand stresses and the value of adhesiveness to other materials (Fan, Wang, Zhang, & Jin, 2017; S. Nam & Mooney, 2021). Different parameters such as chemical, physical, and mechanical factors govern biomaterials' cohesion and adhesion properties, modified by non-covalent and covalent intermolecular interactions. Generally, supramolecular assembly plays a prominent role in improving the cohesive/adhesive properties by entangled polymeric structures, crosslinking with donor-acceptor crosslinking strategy, and metal complexation leading to high adhesive properties even under wet conditions (H. G. Nam, Nam, Yoo, & Kim, 2019) (Bal-Ozturk et al., 2021).

Several chemistries have been used to develop adhesive hydrogels, such as adhesives based on cyanoacrylate (Super Glue) (Cerdá, Ballester, Aliena-Valero, Carabén-Redaño, & Lloris, 2015) and catechol chemistry inspired by mussels foot protein (Bilotto et al., 2019). However, the toxicity and exothermic curing process in cyanoacrylate-based adhesives (Cerdá et al., 2015; García Cerdá, Ballester, Aliena-Valero, Carabén-Redaño, & Lloris, 2015), the neurological effects of dopamine, and the prohibitive cost of catechol functionalized adhesives limit their biomedical applications and clinical practice usage (Jinshan Guo et al., 2018; Schultz, 2007).

Recently, enzyme-mediated crosslinking reactions have gained interest due to the selectivity and versatility of enzyme choices such as transglutaminase (TG), tyrosinase, lysyl oxidase/amine oxidase, thermolysin, and phosphopantetheinyl transferase, etc. (Khanmohammadi et al., 2018; Sakai & Nakahata, 2017). Horseradish peroxidase (HRP)-catalyzed hydrogelation has been a promising candidate for developing bioadhesive hydrogel due to the mild reaction, fast reaction, non-toxicity, and feasibility (Thi, Lee, Le Thi, & Park, 2019). However, the design of bioadhesive using HRP-mediated crosslinking requires catechol groups with limited adhesiveness due to the oxidation of the

catechol groups, as well as the challenge of grafting polymer with a high number of catechol groups. The catechol-modified hydrogel's adhesiveness may decrease due to the catechol groups' occupation with metal ions or oxidation into quinone (Fan et al., 2017).

Plant-derived polyphenols such as tannic acid (TA) with multiple catechol/pyrogallol groups can provide high adhesive to different substrates (both organic and inorganic) as a safe and low-cost molecule (Hao et al., 2020). In addition, due to the presence of multiple hydroxyl groups, TA can form multiple interactions such as hydrogen bonding, hydrophobic, electrostatic, and coordination interactions with a wide range of synthetic and natural materials (Junling Guo, Suma, Richardson, Ejima, & Engineering, 2019; Liang, Zhou, Wu, Li, & Li, 2019). In fact, TA can act as an effective crosslinker both as a primary and secondary network to reinforce the mechanical properties of hydrogels (Bai et al., 2021; Fan, Wang, & Jin, 2018; Lee, Hwang, Kim, & Jeong, 2018; Zhou et al., 2018).

TA-based hydrogels can be either prepared by directly incorporating TA into hydrogel formulation (C. Chen et al., 2021) or indirectly by immersing the hydrogels in TA solution, reinforcing the hydrogel physicochemical and biological properties(Meng et al., 2021). Indirect crosslinking with TA through immersion of the hydrogels in its solution does not interfere with the primary crosslinking, and for that reason, this method has drawn great scientific interest in developing double network (DN) hydrogels. DN hydrogels are a class of interpenetrating polymer network (IPN) materials possessing high mechanical strength and toughness thanks to their unique structure with two high energy dissipation (Haque, Kurokawa, & Gong, 2012). Recently, the production of DN hydrogels through immersion in TA solution has drawn great scientific interest that can provide hydrogels with superior mechanical properties and versatile functions such as adhesiveness and self-healing properties as well as biological activities compared to untreated hydrogels (X. Li et al., 2020; Narasimhan et al., 2021; Wen et al., 2020).

TA cannot be directly used to develop an adhesive hydrogel with HRP-mediated crosslinking due to its strong scavenging effect against H_2O_2 and phenolic radicals, which lead to the inhibition of HRP-mediated crosslinking (Gülçin, Huyut, Elmastaş, & Aboul-Enein, 2010). Thi et al. reported that the

addition of gallic acid to phenol functionalized gelatin hindered the HRP-mediated crosslinking due to the scavenging activity of gallic acid (Le Thi et al., 2020). Hence, to prevent the interfering effect of TA on HRP-mediated crosslinking, the crosslinked hydrogel can be reinforced by immersing in the TA solution.

In this study, for the first time, we developed a series of adhesive hydrogels using the synergy of HRP-mediated crosslinking and TA as a secondary crosslinking. Phenolated chitosan and alginate were used to prepare the hydrogels by the synergy of HRP-mediated crosslinking and electrostatic interaction between chitosan and alginate. Besides, hydrogels were reinforced by TA with different concentrations and pH to investigate the effect of TA reinforcement on hydrogel's physicochemical and mechanical properties. Besides, the TA effect on the hydrogel's biological properties such as antioxidant, antibacterial, and cytocompatibility was evaluated.

2. Materials and methods

2.1. Materials

Chitosan (50-190 kDa) with a deacetylation (DD) degree ≥75% (C3646), sodium alginate (Na-Alg) (W201502, alginic acid sodium salt from brown algae) with molecular weight (Mw) of 120-190 kDa and M/G ratio of 1.61, 1-ethyl-3-(3dimethylaminopropyl)carbodiimide (EDC) (98 %), N-hydroxysuccinimide (NHS) (98 %), horseradish peroxidase (HRP), lysozyme (BioUltra, lyophilized powder, ≥98%, ≥40,000 units/mg protein), 2,2-Diphenyl-1-picrylhydrazyl (DPPH), Hoechst (H33342), ethidium homodimer I (E1903) and hydrogen peroxide (H_2O_2) (30%) were purchased from Sigma Aldrich (St. Louis, MO, USA). 3-(4-Hydroxyphenyl) propionic acid (> 99 %) and tyramine hydrochloride (>98 %) were obtained from Carbosynth (Compton, United Kingdom). Tannic acid, 95% (molecular weight of 1701.23 g mol^{-1}), was purchased from Acros Organics (NJ, USA). The cell Live/Dead assay kit was purchased from Abcam (ab115347, Cambridge, UK).

2.2. Chitosan and alginate modification

Chitosan and alginate were conjugated by phenol groups through reaction with 3-(4-hydroxyphenyl) propionic acid and tyramine, respectively, using carbodiimide coupling chemistry according to our

previous study (Jafari et al., 2022). The conjugation of chitosan-3-(4-hydroxyphenyl) propionic acid (Ch-Ph) and alginate-tyramine (Alg-Ty) was monitored by ^{1}H NMR and Ultraviolet-visible spectroscopy. The phenol content of Ch-Ph and Alg-Ty was measured by Uv-vis spectroscopy using the 3-(4-hydroxyphenyl) propionic acid and tyramine hydrochloride calibration curve at 275 nm. Ch-Ph and Alg-Ty exhibited phenol content of 356 and 280 µmole per gram of polymers, respectively.

2.3. Hydrogel formation

Hydrogels were prepared in two steps; first, the hydrogels were synthesized by enzyme-mediated crosslinking using HRP and H_2O_2, and then they were immersed in TA solution for 24 h to obtain TA reinforced hydrogel. Briefly, phenolated chitosan (Ch-Ph) and alginate (Alg-Ty) were dissolved in deionized water at 1.5 wt%. Then, the solutions were mixed by dropwise addition of the (Alg-Ty) solution to (Ch-Ph) solution under vigorous agitation for one h to homogenize the electrostatic interaction between the positively charged chitosan and negatively charged alginate. Then, the hydrogels were cast into cylindrical molds with a diameter of 30 mm by pouring 2.7 mL gel precursor, followed by the addition of 150 µl HRP and 150 µl H_2O_2 solution with a final concentration of 1 U/mL and 1 mM, respectively. After 10 minutes, the hydrogels were immersed in 20 mL of 10 wt% TA solution at four different pH values of 3, 5.5, 7.4, and 9, and the hydrogels were named Gel-TA pH 3, Gel-TA pH 5.5, Gel-TA pH 7.4, and Gel-TA pH 9. Moreover, four different concentrations of TA solution (1, 10, 20, 30 wt%) at the natural pH of TA solution (3) were used to evaluate the TA concentration on the hydrogel properties, and the hydrogels were named Gel-TA_X, where X refers to the TA solution concentration.

TA loading into the hydrogel influence by immersion media (concentration and pH) was investigated by UV-vis spectrophotometry (Sun, Xiong, Pan, & Cui, 2017). The concentration of the TA solution after immersion was quantified by UV-Vis spectroscopy (LAMBDA™ 25/35 Series UV/vis PerkinElmer spectrophotometer) at 278 nm and a calibration curve of TA with different concentrations.

2.4. Physiochemical characterization

An FT/IR-6600 Spectrometer (JASCO, Japan) at 64 scans per spectrum with a resolution of 4 cm^{-1} was used to record the infrared spectra of freeze-dried hydrogels. Hydrogels swelling index and the enzymatic degradation were investigated using the method previously described (Jafari, Dadashzadeh, et al., 2021; Moshayedi, Sarpoolaky, & Khavandi, 2021). The freeze-dried hydrogels were soaked into a PBS solution at 37 °C for 24 h to obtain the equilibrium swelling. Then, the hydrogels were removed, the excess water was removed by filter paper, and the swelling index (g/g) was calculated using the following equation:

$$Swelling\ index = W_1/W_0 \qquad (1)$$

where W_0 and W_1 are the initial and swelled weight of hydrogels.

The *in vitro* degradation of the Gel-TA hydrogels was evaluated in PBS solution containing 1 mg/ml lysozyme as a degradation media, which was refreshed with new media once per three days (Lungu et al., 2021). The specific weight of the dried hydrogels was immersed into a degradation medium and then incubated in an oven with a temperature of 37℃. At each interval, the hydrogels were taken out from the media and were completely dried in an oven at 50℃ for 72h. The degradation rate was calculated using the following equation:

$$\text{Degradation rate (\%)} = \left(\frac{Wd}{Wi}\right) \times 100 \qquad (2)$$

where W_i and W_d are the initial dried and final weight of hydrogels.

Scanning electron microscopy (SEM) (Hitachi SU-70, Tokyo, Japan) was used to evaluate the microstructure of the cross-sectioned freeze-dried hydrogels.

2.5. TA *in vitro* release

TA release from hydrogel was measured by using UV−Vis spectroscopy according to the described method (Ahmadian et al., 2021). The influence of the concentration and pH of immersion media on the release of TA in PBS was evaluated. Hydrogels at different pH (3, 5.5, 7.4, and 9) at a constant

TA concentration (10 %), and hydrogels with different TA concentrations (0, 1, 10, 20, and 30 %) at constant pH (3) were used to study the TA release. Briefly, 0.1 g of the dried hydrogels were immersed in 20 mL of PBS and placed into a shaker incubator at 100 rpm at 37℃. Then, 1 mL of the hydrogels' release media at pre-determined time points was withdrawn and replaced with 1 mL of fresh PBS solution to maintain the total volume of release medium constant (20mL). After sampling in the time points, the cumulative concentration of released TA from hydrogels was quantified according to the calibration curve and UV-Vis spectroscopy at 278 nm. (n=3)

2.6. Rheological properties

The rheological behavior of hydrogels was investigated using a rheometer (Anton Paar MCR 302, Austria) equipped with a plate-plate geometry (25 mm) at 37 ℃. Storage modulus (G') and loss modulus (G'') of hydrogels were evaluated using oscillatory tests (He et al., 2020). The frequency sweep test was conducted at a frequency range from 0.1 to 100 Hz and a constant strain of 0.1 %. Besides, an amplitude sweep test (1 to 500 %) was performed at a constant frequency of 1 Hz (Jing et al., 2019).

2.7. Thermal properties

The thermal stability of Gel-TA hydrogels was evaluated by thermogravimetric analysis (TGA-DTA) analysis using a TA instrument (Netzsch STA 409 PC coupled with Netzsch QMS 403C). Freeze-dried hydrogels (30 mg) were heated from 30 ℃ to 600 ℃ at a heating rate of 10 ℃/min under nitrogen flow (60 mL/min).

2.8. Adhesiveness assessment

Hydrogels adhesiveness was evaluated by lap shear test using Zwick/Roell Z020 universal testing machine (Zwick GmbH, Ulm, Germany) according to the method described (He et al., 2020). Briefly, the hydrogels were formed by enzyme-mediated crosslinking on the two opposite sides of porcine skin (2×3 cm) with 5 mm thickness, and two porcine skin pieces were bonded. Then the samples were immersed in TA solution (1, 10, 20, 30 %) for 24 h prior to the experiment. Then, the incubated

samples were tested via lap shear test with a 2kN cell load at a constant speed of 10 mm/min until the breakage of attached porcine skins to obtain the adhesive strength of the samples. (n = 3).

2.9. Antioxidant activity

The antioxidant activity of hydrogels was investigated by DPPH[1] radical scavenging assay (Tran, Le Thi, Thi, & Park, 2020). Briefly, the hydrogels were incubated into 1 mL DPPH solution (0.5 mM) in a 48-well plate for 30 min in the dark. Then, the absorbance of hydrogels and control (100 µL distilled water) at 520 nm was measured using a microplate reader (Epoch microplate, BioTek Instruments, Inc., Winooski, VT, USA). The DPPH radical scavenging activity (%) was measured using the following equation:

$$\text{Radical scavenging activity } (\%) = [1 - (As/Ac)] \times 100 \quad (3)$$

Where A_s and A_C are the absorbances of samples, and the control (distilled water), respectively.

2.10. Antibacterial performance

The antibacterial activity of hydrogels was investigated against Gram-negative *Escherichia coli* (*E. coli*, ATCC 27195) and Gram-positive *Staphylococcus aureus* (*S. aureus*, ATCC 25923) using a disk diffusion test (Rezaei et al., 2020). Briefly, one single-cell colony of freshly cultured bacteria was inoculated into Muller-Hinton (M–H) broth and incubated at 37 °C to reach an absorbance value of 0.5 McFarland equivalent turbidity standard (10^8 CFU/mL). Then, agar plates were uniformly spread with 100 µL of the bacterial suspension (10^6 CFU/mL). The cylindrical discs hydrogels were placed onto an agar plate and incubated for 24 h at 37 °C. The antibacterial effect of the hydrogels was measured by the inhibition zone around each sample (n=3).

2.11. Cytocompatibility

The cytocompatibility of hydrogels was evaluated using 3T3-L1 mouse fibroblast cells by MTS and a live/dead assay (Chan et al., 2020; F. Wang et al., 2020). The hydrogels were transferred to a 96-well plate and sterilized by washing with PBS (2 times), then exposed to ultraviolet light for 30 minutes

[1] 2,2-diphenyl-1-picryl-hydrazyl-hydrate

(Kumar, Nune, & Misra, 2018). Then, 3T3-L1 cells with a cell density of 10^4 cells/well were seeded on the hydrogel and incubated for three days, and the media was replaced every day. At one and three days, 20 µL of MTS solution was added to the wells and incubated for four h. After incubation, the media was transferred to a 96-well plate, and the cell viability was evaluated by measuring the absorbance of the control (cell-cultured media) and the samples at 490 nm using a plate reader (n=3).

For the live/dead staining, the sterile hydrogels were placed into a Millicell EZ SLIDE 8-well glass (Merck, Kenilworth, NJ, USA), and the cells with a density of 10^4 cells/well were seeded on the hydrogels. According to the manufacturer's instructions, the cells were stained using the live/dead kit. Live cells were stained green and dead cells red, and the images were taken using a fluorescent microscope (Zoe fluorescent cell imager, Biorad, Hercules, CA).

Moreover, the hydrogel cell distribution was evaluated by nucleus staining using Hoechst 33258 (Rivero et al., 2020). Briefly, the cell-seeded hydrogels were cultured for three days at 37 °C, and the cell nucleus was stained using 10 µM Hoechst and incubated for 45 min. After washing the cells with PBS two times, the cells were fixed using 4% paraformaldehyde. The cell nuclei distribution and morphology were analyzed using a fluorescent microscope (Zoe fluorescent cell imager, Biorad, Hercules, CA).

2.12. Statistical analysis

All experiments were carried out in triplicates, and the results were expressed as means ± standard deviations. Statistical analyses were performed using GraphPad Prism 8 (GraphPad Software Inc.) using one-way ANOVA followed by Tukey's posthoc analysis. P-values < 0.05 were considered statistically significant. Wherever significance has been proven, it is indicated by $*p < 0.05$.

3. Result and discussion

3.1. Hydrogel fabrication

The Gel-TA hydrogels were fabricated in two-step methods; first, the enzymatic crosslinking of phenolated chitosan and alginate hydrogel was followed by TA reinforcement by incubation in TA solution (Scheme 1). First, the chitosan and alginate were conjugated with phenol groups using a

carbodiimide coupling chemistry (Fig 1a), and the ^{1}H NMR spectra of Ch-Ph and Alg-Ty demonstrated new signals around 6.6-7.2 ppm corresponding to the aromatic ring protons of the phenol groups showing the successful conjugation of phenol groups to the backbone of chitosan and alginate (Fig 1b,c) (T. Li et al., 2019). Moreover, the new peaks presented at 1.1, 2.8, and between 3-3.5 ppm in Alg-Ty spectra are due to the residual EDC–urea byproduct after the amide coupling reaction (Jeon et al., 2009; Sandvig et al., 2015). Besides, unlike the unmodified chitosan and alginate, the presence of a new peak at 275 nm in the UV spectra Ch-Ph, and Alg-Ty could confirm the phenol modification (Fig 1 d,e) (Sakai et al., 2018). Then, the mixture of Ch-Ph, and Alg-Ty at the concentration of 1.5 % (1:1 volume ratio) solution was used for the hydrogel formation by HRP-mediated crosslinking. The hydrogel was formed immediately after adding HRP and H_2O_2 due to the catalysis of oxygen radicals generated by HRP/H_2O_2 leading to the formation of C-C and C-O bonds between the phenoxy radicals (Liu et al., 2020).

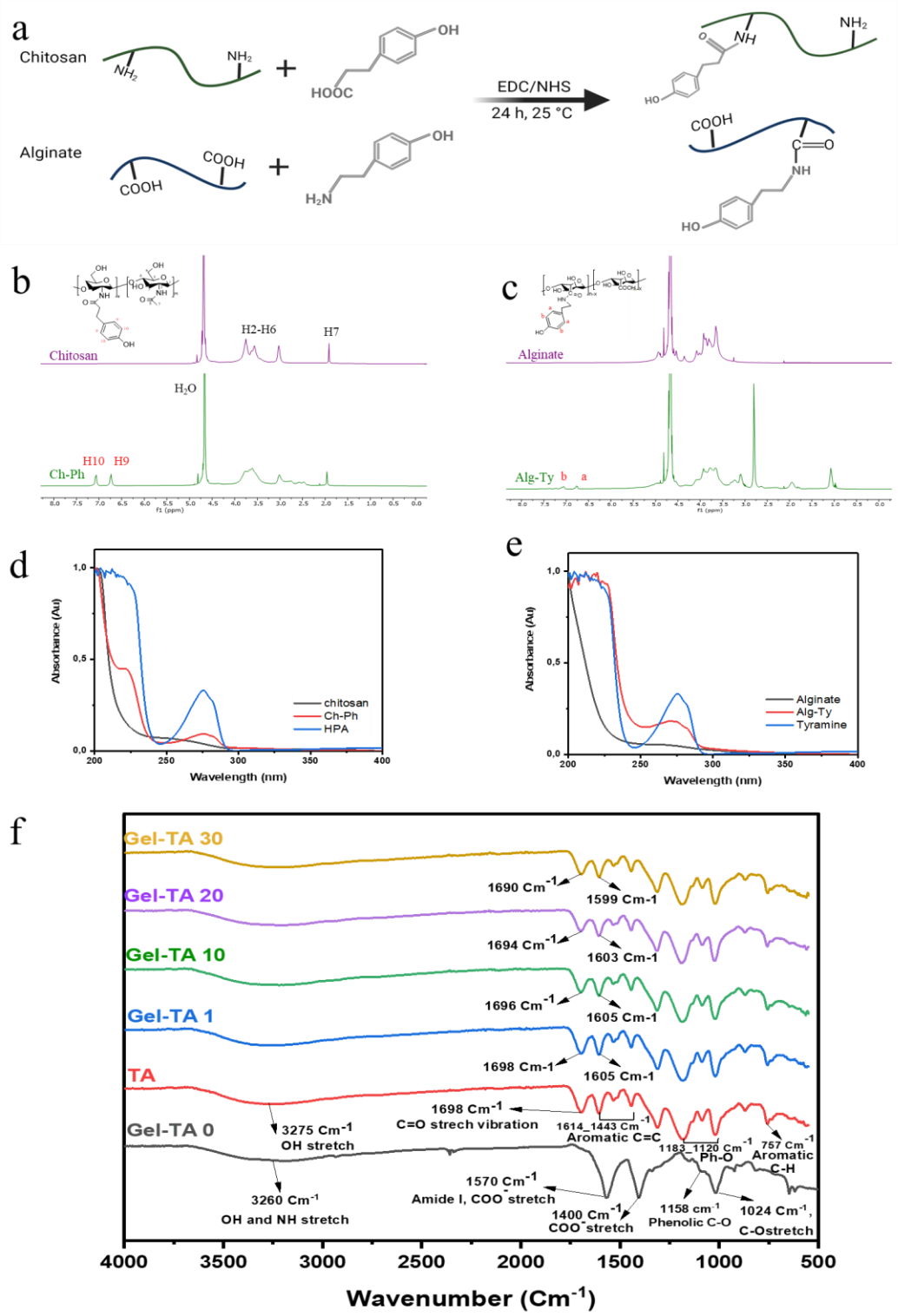

Figure 1. a) Schematic illustration of phenol conjugation to the chitosan and alginate backbone; b) ^{1}H NMR spectra of the Ch-Ph conjugate and unmodified chitosan; c) ^{1}H NMR spectra of the Alg-Ty conjugate and unmodified alginate; d)UV-vis spectra of Ch-Ph, unmodified chitosan, and 3-(4-hydroxyphenyl) propionic acid

(HPA); e) UV-vis spectra of Alg-Ty, unmodified alginate, and tyramine; f) FTIR spectra of TA and Gel-TA hydrogels.

In the second step, the enzyme-mediated crosslinked hydrogel was immersed into a TA solution to obtain TA reinforced hydrogel (Gel-TA) through the formation of secondary crosslinking. After immersion, the hydrogel color changed to light brown, indicating the TA incorporation and formation of secondary crosslinking (Kaczmarek-Szczepańska, Mazur, Michalska-Sionkowska, Łukowicz, & Osyczka, 2021). TA can form multiple interactions such as hydrogen bonding, hydrophobic, electrostatic, and coordination interaction with a wide range of polymers (Junling Guo, Suma, Richardson, & Ejima, 2019). In this study, hydrogen bonding is formed between multiple hydroxyl groups of TA, with hydroxyl, amine groups of chitosan (An, Kang, & Li, 2019), and carboxyl groups of alginate (W. Zhang et al., 2020). Moreover, a weak electrostatic interaction can be formed between protonated amino groups of chitosan and ionized phenoxy hydroxyl groups of TA (An et al., 2019) (Scheme 1).

To investigate the chemical bonds of Gel-TA hydrogels, FTIR was performed (Fig 1f). We previously showed that enzymatically crosslinked phenolated chitosan-alginate revealed a similar FTIR spectrum compared to the individual chitosan and alginate hydrogel with a shift in the carboxylate groups of alginate. Besides, the amide I band of chitosan disappeared and overlapped with the carboxylate groups of alginate, indicating the formation of electrostatic interaction between the positively charged chitosan and negatively charged alginate (Jafari et al., 2022). The broad peak at 3260 cm^{-1} is attributed to the OH and NH stretch, and the sharp peak at 1570 corresponds to the amide I of chitosan and carboxylate stretch of alginate, which overlapped due to the electrostatic interaction (Ho, Mi, Sung, & Kuo, 2009).

Moreover, the peaks at 1400 and 1024 cm^{-1} are associated with the carboxylate and C-O stretch of alginate. Besides, the peak at 1158 cm^{-1} is attributed to the phenolic C-O band presented in Gel-TA 0 due to the phenol conjugation (Kim, Kim, Song, Kang, & Park, 2020). The TA spectrum showed the stretching vibration of the phenolic (-OH) group between 3500 and 3000 cm^{-1}, and a peak at 1698 is attributed to the stretching vibration of C=O groups of carboxylic ester (Ge et al., 2019). The peaks at

1614-1443 cm^{-1} correspond to the aromatic C=C stretch, and the characteristic peaks at 1183-1120 and 757 cm^{-1} are attributed to the substituted benzene ring vibration and bending aromatic vibration C–H of TA (He et al., 2020). For the TA reinforced hydrogels (GEL-TA 1, 10, 20, and 30), all the characteristic peaks of TA were observed, indicating the successful TA incorporation into the hydrogels. Furthermore, after the TA treatment, the characteristic peaks of amide I and carboxylate stretch of Gel-TA 0 at 1570 cm^{-1} was disappeared and overlapped with the aromatic C=C stretch bands of TA at 1605 cm^{-1}, possibly due to the hydrogen bonding between hydroxyl groups of TA, the amine groups of chitosan, and carboxyl groups of alginate (Božič, Gorgieva, & Kokol, 2012). Moreover, the amide I and carboxylate stretch of Gel-TA hydrogels were shifted to a lower wavenumber (from 1605 to 1599 cm^{-1}), showing the enhancement of hydrogen bonding by increasing the TA concentration from 1 to 30 %. Besides, the characteristic peaks of C=O groups of TA was shifted to the lower wavenumber (1698 to 1690 cm^{-1}) after TA treatment by increasing TA concentration from 1 to 30 % which could be due the possible hydrogen bonding between hydroxyl groups of TA and amine and carboxyl groups in chitosan-alginate hydrogel.

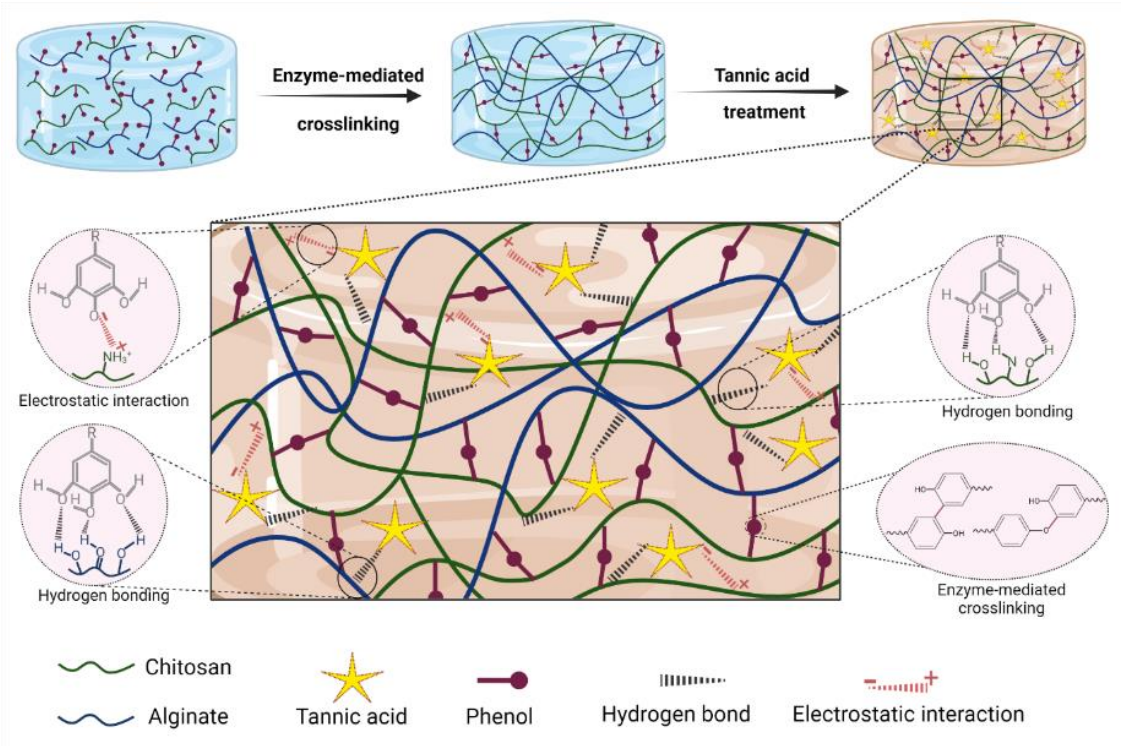

Scheme 1. Schematic illustration of Gel-TA preparation through the enzyme-mediated crosslinking and subsequent tannic acid reinforcement and the possible interaction between TA, chitosan, and alginate.

3.2. Effect of pH and TA concentration on TA interaction

First, we investigated the effect of pH on the TA conjugation due to the pH sensitivity of TA interaction (Abouelmagd, Abd Ellah, Amen, Abdelmoez, & Mohamed, 2019). At a constant TA concentration (10 %), three different pH (5.5, 7.4, and 9), in addition to the TA solution natural pH (3) were investigated. The TA reinforced hydrogels exhibited a different surface and roughness, as well as different TA loading by changing the TA solution pH. Increasing pH up to 7.4 increased the TA loading from 30.8 ±2.4 to 86.1 ± 2.3 mg/g and further increased to pH 9, resulting in a significant decrement in TA loading (3.5 ± 0.9 mg/g).

The TA loading results show pH's significant effect on the polymer/TA interactions. The protonation or ionization of TA depends on the solution pH (pKa~8.5 for TA), which further affects the interaction between polymer and TA (I Erel-Unal & Sukhishvili, 2008). At acidic conditions, the phenol groups of TA are mainly protonated, which are hydrogen donors for binding with hydrogen-accepting chitosan and alginate but have weak electrostatic interaction with cationic chitosan (T. Shutava, Prouty, Kommireddy, & Lvov, 2005; T. G. Shutava & Lvov, 2006). Increasing the pH significantly enhanced the electrostatic interaction between deprotonated phenolic hydroxy groups on TA and the free amino groups of chitosan, leading to an increase in TA loading and crosslinking density. Moreover, the water loss of hydrogel after immersion showed that by increasing the pH to 7.4, the water loss increased from 73.1 ± 1.9 to 90.6 ± 1.4 %, and the hydrogels at pH 5.5 and 7.4 were completely dehydrated with high shrinkage after 24 h immersion. However, the minimum loading (3.5 ± 0.9 mg/g) and water loss (45.9 ± 4.4) occurred at pH 9, possibly due to the oxidation of TA molecules resulting in the TA self-assembly, which hinders TA from interacting with the hydrogel (Zhan, Yan, Sheng, & Li, 2020).

Then, at the natural pH of TA solution (3), the effect of TA concentration was investigated on the hydrogel properties. The results showed an increase in TA loading from 8.1 ± 1.2 to 241 ± 27.1 mg/g

by increasing the TA concentration (1 to 30 %), indicating the formation of more interaction between the hydrogel and higher crosslinking density. Moreover, the same trend was observed for the hydrogels' water loss, and the Gel-TA 30 exhibited the maximum water loss (86.6 ± 1.7 %), while the Gel-TA demonstrated the lowest amount of water loss (52.3 ± 3.8 %).

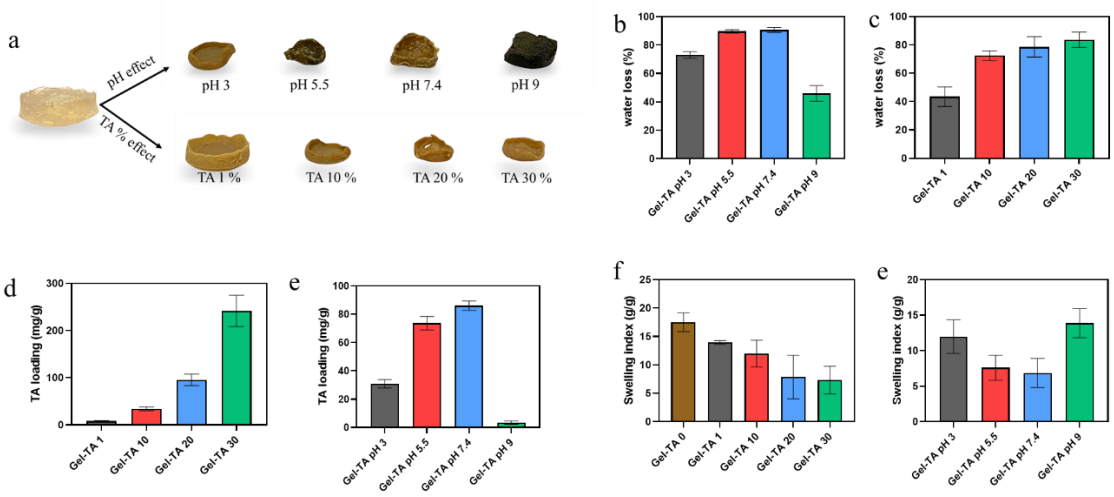

Figure 2. a) photograph image of hydrogels after immersion in TA solution with different pH (3, 5.5, 7.4, 9) at a constant concentration of TA (10 %) and TA solution with different concentrations (1, 10, 20, 30 %) at constant pH 3 (natural pH of TA solution); b) water loss of hydrogel after 24 h immersion in TA solution with different pH at a constant concentration of TA (10 %); c) water loss of hydrogel after 24 h immersion in TA solution with different concentrations (1, 10, 20, 30 %) at constant pH 3; d) TA loading onto the hydrogels treated with different pH (3, 5.5, 7.4, 9) of TA solution at a constant concentration of TA (10 %); e) TA loading onto the hydrogels treated different TA solution concentration (1, 10, 20, 30 %) at constant pH 3.

3.3. Swelling behavior

The swelling index of Gel-TA hydrogels treated with different pH and TA concentrations was evaluated (Figs 2f,e). The results demonstrated that increasing TA loading reduced the swelling index due to the secondary crosslinking and, subsequently, increased crosslinking density (Gwak, Hong, & Park, 2021). Among the hydrogel treated with different pH of TA solution, Gel-TA pH 7.4 exhibited the lowest swelling index (6.85 ± 1.4 g/g), while Gel-TA pH 9 showed the highest swelling index (13.8 ± 1.5 g/g) (Fig 2e). Moreover, increasing the TA concentration from 1 to 30 % decreased the hydrogel's swelling index; therefore, the swelling index decreased from 13.9 ± 1.1 to 7.3 ± 1.7 g/g,

while the untreated hydrogel (Gel-TA 0) demonstrated the highest swelling index (17.4 ± 1.7) among the samples. The results showed that TA treatment could significantly decrease the swelling capacity of the hydrogel due to the formation of secondary crosslinking via hydrogen bonding between TA and the chitosan and alginate network (He et al., 2020).

3.4. Microstructure, *in vitro* TA release, and degradation behavior of hydrogels

The microstructure of hydrogels was evaluated by scanning electron microscopy (SEM) (Fig 3a), and the results showed a microporous morphology for all of the hydrogels regarding the TA concentration. However, increasing TA concentration caused a reduction in the pore size of hydrogel and led to a more compact structure with smaller pores compared to the untreated hydrogel. The result is in agreement with the swelling capacity, which lower swelling was due to the smaller pore size and denser hydrogel microstructure. This phenomenon is due to the crosslinking effect of TA, and increasing the TA concentration, augments the crosslinking density of hydrogel because of a high amount of hydrogen bonding between TA and the polymer chains (X. Li et al., 2020).

Besides, the *in vitro* TA release of hydrogels treated with different pH and concentrations of TA solution were investigated using UV spectrophotometry (Figs 3b,c). First, the effect of varying pH of immersion media was investigated on the TA release (Fig 3b), and the results demonstrated that by increasing the pH from 3 to 7.4, the TA release after 72 h increased from 1239.5±22.1 to 1874.8±43.2 ppm; while, minimum TA release was observed for pH 9 (447.4±53.4), which is aligned with the TA loading result agreeing with the lowest TA loading at pH 9. Moreover, an assessment of the TA concentration effect on the TA release revealed that increasing TA concentration caused an augmentation in the release profile of TA due to the higher loading of TA on the hydrogels than the hydrogels in the presence of a lower concentration of TA. All samples showed a burst release during the first hour, which could be due to the presence of poorly bonded TA on the surface of the hydrogel that quickly transferred to the PBS media. Similarly, burst release of unbounded and poorly crosslinked TA at one h of immersion into PBS has been reported previously (Z.-Y. Zhang et al., 2020).

Furthermore, the enzymatic degradation behavior of the hydrogels treated with different pH and concentrations of TA were investigated in lysozyme solution at 37 °C (Figs 3d,e). The results showed that changing the TA solution pH significantly affects the hydrogel's degradation. By increasing of samples' pH from 3 to 7.4, their degradation rate decreased so that the ultimate remaining mass of Gel-TA pH 3 and 7.4 was 13. 1 ± 0.5 and 59.6 ± 2.1 %, respectively. However, further increasing to pH 9 caused an acceleration in the hydrogel degradation with the lowest remaining mass (9.7 ± 1.2 %). The results showed that the formation of ionic interaction at pH 5.5 and 7.4 could significantly slow down the degradation rate in comparison to pH 3 which hydrogen bonding is the primary interaction between the TA and the polymer chain. The slow degradation rate of samples with higher pH is due to the stronger ionic bonds than the hydrogen bond, which decreased the degradation rate.

Moreover, by increasing the TA concentration from 1 to 30% at the same pH (3), the degradation rate decreased due to the formation of a higher amount of hydrogen bonding and crosslinking density (Fig 3e). It is worth mentioning that the untreated hydrogel (Gel-TA 0) was completely degraded after 10 days (data are not shown), indicating the significant effect of TA on the hydrogel degradation, which prolonged the degradation rate from 10 days to more than 50 days. TA inhibits the lysozyme activity by bonding with the active sites of lysozyme via hydrogen bonding, hydrophobic, and ionic interaction, which leads to lysozyme aggregation (Su et al., 2019). Hence, several factors contributed to the enhanced degradation resistance of the Gel-TA hydrogels, including TA's inhibitory effect on the enzyme and its crosslinking capability.

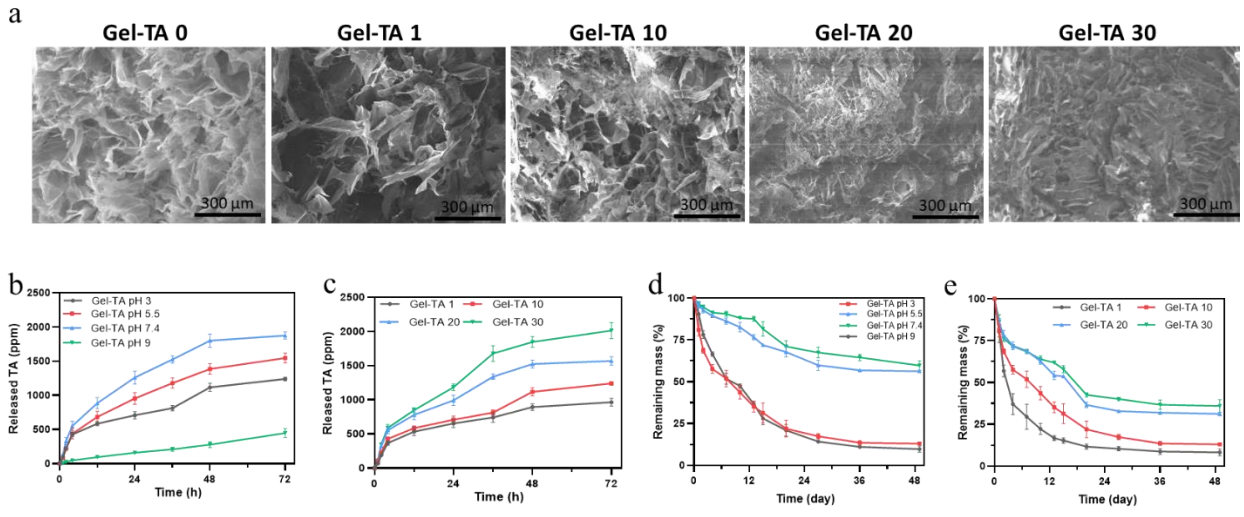

Figure 3. a) Gel-TA hydrogels microstructures; b,c) TA release of hydrogels treated with different pH and TA concentration; d,e) degradation profile of Gel-TA hydrogel treated with different pH and TA concentration.

3.5. Viscoelastic properties of Gel-TA hydrogels

The effect of TA treatment on hydrogels' stiffness and viscoelastic properties was assessed by rheological measurement (Fig 4). The Gel-TA 0 hydrogels demonstrated a storage modulus (7 kPa) independent of frequency due to the covalent and non-reversible nature of enzymatic crosslinking (Fig 4a) (McGill, Coburn, Partlow, Mu, & Kaplan, 2017). TA treatment increased the G' of hydrogels, and increasing TA content from 1 to 30 %, significantly improved the G' of hydrogels from 14 to 40 kPa (Figs 4a,b) (at a frequency of 1 Hz), due to the formation of secondary crosslinking through the hydrogen bonding between TA, and functional groups of chitosan and alginate. Moreover, Gel-TA 1 exhibited a G' frequency-dependent compared to Gel-TA 0; besides, the G' frequency-dependent behavior was intensified in Gel-TA 10, 20, and 30 (Fig 4b). This phenomenon is due to the formation of new non-covalent bonds such as hydrogen bonding and electrostatic interaction with dynamic nature between hydroxyl groups of TA, hydroxyl, and amine groups of chitosan, as well as carboxyl and hydroxyl groups (Hossain et al., 2020; Ross-murphy, 1995). Indeed, restriction of polymer chain movement at high frequency leads to the higher G', indicating that TA treated hydrogels had a more viscoelastic behavior compared to the Gel-TA 0 (Lee et al., 2018).

Furthermore, TA treatment caused a significant tan delta (Tan δ= G'/G") increment from 0,04 to 0.4 at a frequency of 1 Hz (0 to 30 % TA), indicating that non-covalent interaction could improve the energy dissipation of hydrogel during the deformation due to the reversible nature of hydrogen bonding (Hao et al., 2020).

The amplitude sweep results (Figs 4c,d) showed that increasing TA concentration (0 to 30 %) could improve both G', and G' compared to the Gel-TA 0. Besides, similar to the frequency sweep test, Gel-TA hydrogel (Fig 4c,d) demonstrated a different behavior compared to the non-treated hydrogel (Gel-TA 0) (Fig 4c). Indeed, Gel-TA 0 showed a sharp reduction in G' after the linear viscoelastic region

(LVR); however, the TA reinforced hydrogel showed a lower slop reduction in G', showing the elastic behavior could be due to the presence of dynamic non-covalent bonding. Viscoelastic assessment results confirmed TA's role as a secondary crosslinking, which led to a transition from elastic to more viscoelastic behavior (K. Chen et al., 2021).

3.6. Thermal properties of the Gel-TA hydrogels

Thermogravimetric analysis (TGA) was performed to investigate the effect of TA treatment on the thermal stability of the hydrogels (Figs 4e,f). The thermal degradation showed two decomposition stages for all of the hydrogels. The first stage occurred between 50-150°C with minor weight loss of approximately 10% due to the water evaporation of hydrogels (Table 1) (Yang et al., 2019). The second decomposition stage happened at 200-300 °C with a sharp weight loss corresponding to the polysaccharides chain degradation (Jafari, Delporte, et al., 2021). By increasing TA content from 0 to 30 %, the maximum degradation temperature was not significantly changed; however, Gel-TA 20, and 30 exhibited extra DTGmax at 278.5 and 286.5 °C, respectively (Fig 4f). This phenomenon might be due to the presence of higher amount of TA into the Gel-TA20, and Gel-TA 30 compared to Gel-TA 1, and Gel-TA 10. Moreover, Nam *et al*. have shown that the pure TA exhibited a DTGmax at 292 °C indicating that the second DTGmax of Gel-TA20, and Gel-TA 30 belongs to the TA decomposition (H. G. Nam et al., 2019).

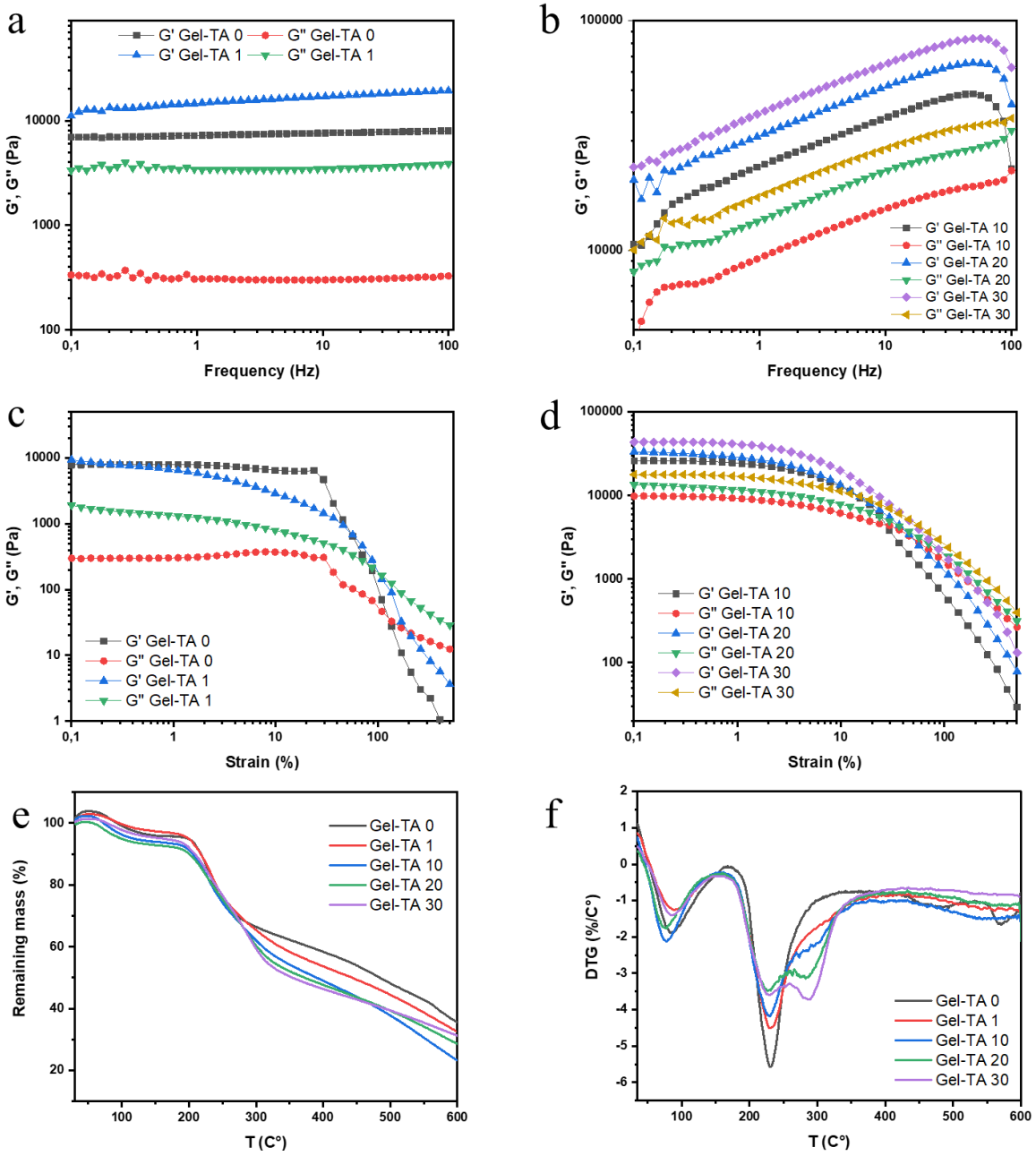
a
G' Gel-TA 0
G" Gel-TA 0
G' Gel-TA 1
G" Gel-TA 1
G', G" (Pa)
Frequency (Hz)
b
G' Gel-TA 10
G" Gel-TA 10
G' Gel-TA 20
G" Gel-TA 20
G' Gel-TA 30
G" Gel-TA 30
G', G" (Pa)
Frequency (Hz)
c
G' Gel-TA 0
G" Gel-TA 0
G' Gel-TA 1
G" Gel-TA 1
G', G" (Pa)
Strain (%)
d
G' Gel-TA 10
G" Gel-TA 10
G' Gel-TA 20
G" Gel-TA 20
G' Gel-TA 30
G" Gel-TA 30
G', G" (Pa)
Strain (%)
e
Gel-TA 0
Gel-TA 1
Gel-TA 10
Gel-TA 20
Gel-TA 30
Remaining mass (%)
T (C°)
f
Gel-TA 0
Gel-TA 1
Gel-TA 10
Gel-TA 20
Gel-TA 30
DTG (%/C°)
T (C°)

426

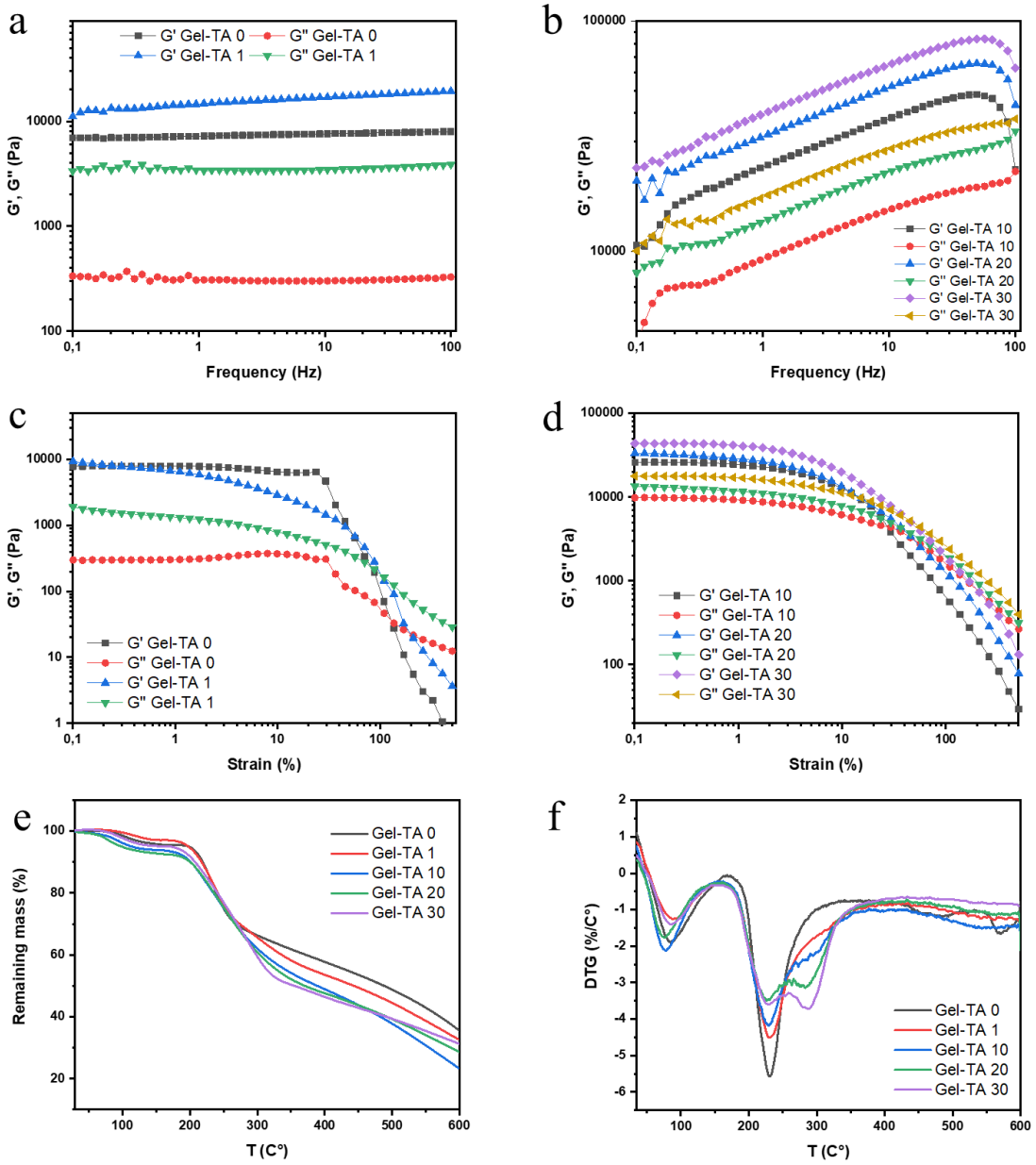

427

428 **Figure 4.** Rheological and thermal properties of the Gel-TA hydrogels. a,b) storage modulus (G') and loss
429 modulus (G")–frequency dependence of Gel-TA hydrogels at a constant strain of 1% at 37 °C; c,d) storage
430 modulus (G') and loss modulus (G")–strain dependence of Gel-TA hydrogels at a constant frequency of 1 Hz at
431 37 °C; e) TGA curve of Gel-TA hydrogels; f) DTG curve of Gel-TA hydrogels.

432

433

434

435 Table 1. Thermal properties of Gel-TA hydrogels.

Sample	First stage degradation			Second stage degradation		
	Range (°C)	Peak (°C)	Weight loss (%)	Range (°C)	Peaks (°C)	Weight loss (%)
Gel-TA 0	50-150	85.1	8.9	200-300	229.1	59.3
Gel-TA 1	50-150	87.8	7.5	200-300	229.8	63.8
Gel-TA 10	50-150	78.6	9.3	200-300	229.5	69.6
Gel-TA 20	50-150	77.1	7.9	200-300	225.8- 278.5	64.1
Gel-TA 30	50-150	85.6	6.5	200-300	229,2- 286.5	63.1

436

437 **3.7. Adhesion behavior of Gel-TA hydrogels**

438 The adhesiveness of the Gel-TA hydrogels was investigated by a lap shear test using porcine skin as a
439 substrate (Fig 5). The hydrogels were injected between two pieces of porcine skin and then treated
440 with different concentrations of TA (Fig 5a). The adhesion strength was determined by measuring the
441 maximum adhesion strength during the detachment (Fig d). The Gel-TA 0 hydrogel (without
442 treatment) did not show any adhesiveness to the porcine skin; however, the hydrogels could attach to
443 the porcine skin after TA treatment. Besides, increasing the TA content from 1 to 30 % improved the
444 adhesive strength of hydrogels from 1.4 ± 0.3 to 16.1 ± 0.1 kPa (Fig 5e), showing the significant
445 effect of TA in enhancing the adhesiveness of hydrogel to the biological tissue. In addition to the
446 biological tissue (porcine skin), the hydrogel (Gel-TA 30) could be attached to different substrates
447 such as plastic, glass, and metal, showing its adhesiveness to a wide range of materials (Fig 5b).
448 Previous studies reported a significant effect of TA on the adhesiveness of hydrogels to the different
449 substrates due to the presence of 25 hydroxyl groups in the pyrogallol and pyrogallol ester groups of
450 TA, which leads to the formation of dense hydrogen bonding with various substrates from biological
451 tissues to metallic materials (Fan et al., 2017). Depending on the substrates, different mechanisms can
452 be considered for the adhesiveness of TA-based biomaterials. For example, H-bonding, π-π stacking,
453 and hydrophobic interaction are responsible for the attachment of TA-based hydrogel to wood;
454 however, metal coordination is mainly accountable for attachment to the stain steel. In the case of
455 biological tissues, TA can also provide adhesion via the interaction of its catechol-free groups with
456 amine or thiol groups (from peptides and proteins) on the tissue surface (Fig 5f) (Han et al., 2017).

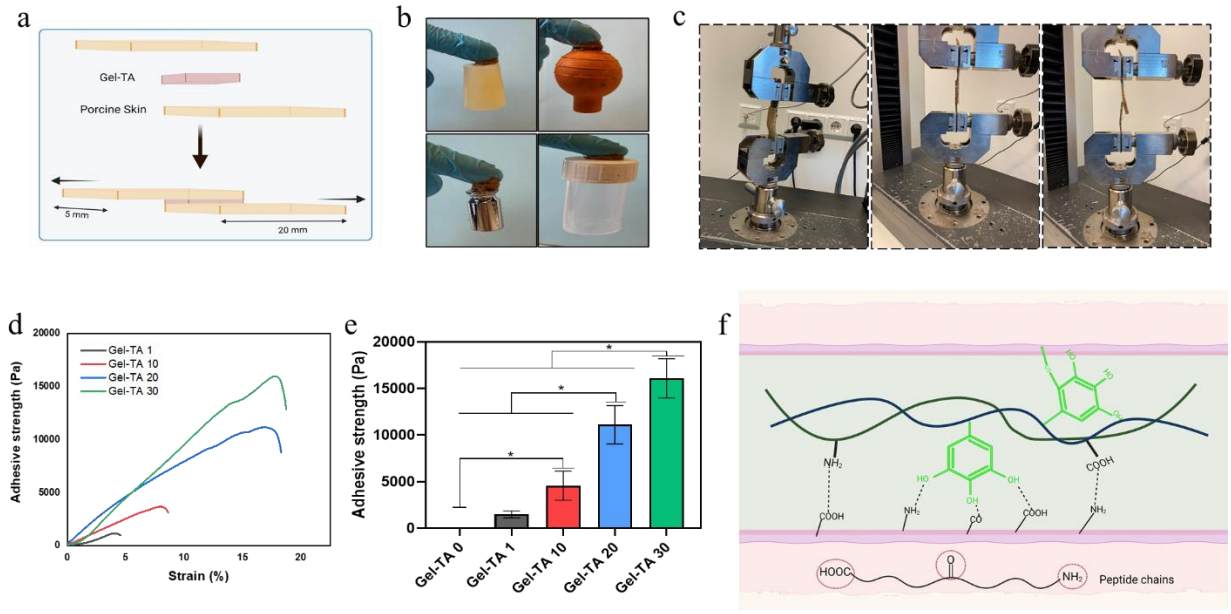

457

458 **Figure 5.** Adhesive properties of Gel-TA hydrogels. a) Schematic illustration of sample preparation of lap shear
459 test; b) photographs Gel-TA adhesion to various substrates such as metal and plastic; c) Photographs of lap-
460 shear tests of two porcine skin adhered with Gel-TA hydrogel; d) stress-strain curve the lap shear test on Gel-
461 TA hydrogel; e) The adhesive strength of Gel-TA hydrogels. Data were analyzed using a one-way ANOVA test,
462 $*p < 0.05$ as a compared type of hydrogel; f) The possible adhesiveness mechanism of gel-TA hydrogels to the
463 biological tissue.

464 ### 3.8. Antioxidant and Antibacterial properties of Gel-TA hydrogels

465 The antioxidant activity of Gel-TA hydrogels was investigated by determining their capability to
466 scavenge (Fig 6a). TA treatment significantly improved the antioxidant activity of the hydrogel. The
467 DPPH scavenging activity of Gel-TA 0 was 36.8 ± 2.5 % due to the intrinsic antioxidant activity of
468 chitosan; however, the TA treated hydrogels demonstrated a DPPH scavenging activity of above 96 %
469 due to the high antioxidant activity of TA. Indeed, TA contains gallol and catechol groups with
470 multiple hydroxyl groups responsible for its high antioxidant activity by the resonance stabilization of
471 delocalized electrons (Gwak et al., 2021). Moreover, a complete decolorization of DPPH solution
472 from purple to yellow was observed for the Gel-TA hydrogels sample indicating a complete pairing of
473 an electron with hydrogen atoms of TA and the formation of reduced DPPH (Fig 6b) (Ge et al., 2019).

No significant difference in the DPPH scavenging activity was observed between TA-treated hydrogels due to the fast release of the required amount of TA for the scavenging effect.

Tannic acid demonstrates antibacterial activity against both Gram-positive or Gram-negative bacteria by several mechanisms. TA can penetrate the cell membrane of bacteria, interfere with cell metabolism, and demolish bacteria growth. Moreover, TA can hinder bacteria from attaching to the surface, which leads to bacteria cell death due to the lack of attachment. TA's ability to inhibit sugar and amino acids is another feature that contributes to the antibacterial activity of TA (Kaczmarek, 2020; Pandey & Negi, 2018). The antibacterial activity of the Gel-TA hydrogels against Gram-positive (*S. aureus*) and Gram-negative bacteria (*E. coli*) was evaluated using the disk diffusion method (Fig 6c). The antibacterial activity of Gel-TA 0 hydrogel was improved after TA treatment according to the bigger inhibition zone in TA treated hydrogels. Besides, by increasing TA content from 1 to 30, the inhibition zone was slightly increased against *E. coli* and *S. aureus*, indicating TA concentration's effect on the antibacterial activity.

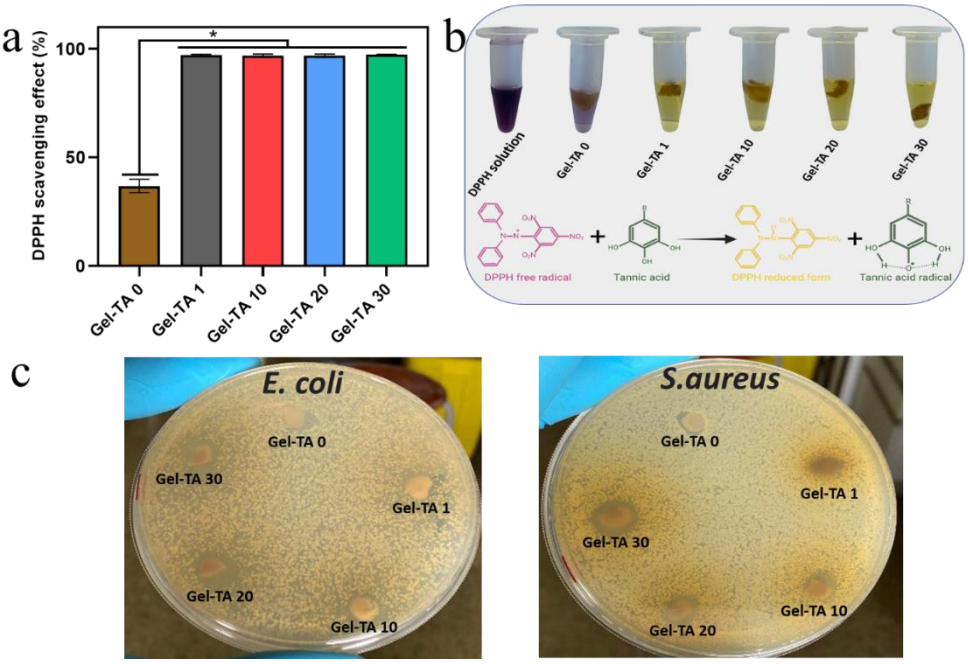

Figure 6. a) The DPPH scavenging activity of Gel-TA hydrogels, results are expressed as % scavenging activity and are the mean ± SD of three independent experiments. Data were analyzed using a one-way ANOVA test, *$p < 0.05$ as a compared type of hydrogel; b) photographs of Gel-TA hydrogels incubated with DPPH solution

for 50 min, and the scavenging mechanism of TA; c) antibacterial activity of Gel-TA hydrogels against *E. coli*, and *S. aureus* investigated by disk diffusion method.

3.9. Cytocompatibility of Gel-TA hydrogels

The cytocompatibility of hydrogels was investigated by live/dead and MTS assay using 3T3-L1 mouse fibroblast cells (Fig 7). The MTS assay showed a good cytocompatibility for the hydrogel with no less than 80 % viability after 24 and 72 h, indicating the non-toxicity nature of the hydrogels (Fig 7b). The Gel-TA 0 and Gel-TA 1 showed lower viability compared to the control sample (cell culture media). The results indicated that TA treatment had no toxic effect on the cell viability of fibroblast cells (Taheri, Jahanmardi, Koosha, & Abdi, 2020).

Moreover, live/dead staining (Fig 7a) showed a high number of vial cells (green) in comparison to the dead cells (red), indicating the cytocompatibility of hydrogel. Moreover, both live/dead and nucleus staining showed that the cells seeded on Gel-TA 0 and Gel-TA 1 exhibited a round morphology with a tendency to cell cluster; however, by increasing TA concentration, the hydrogels demonstrated cell spreading distribution (Fig 7a). This phenomenon could be due to improving hydrogels hydrophilicity resulting from TA treatment (Xinyu Hu, Wang, Zhang, & Xu, 2017; R. Wang et al., 2019).

Hence, TA treatment has not shown any adverse effect on fibroblast cells' cell viability and proliferation and could induce cell proliferation. Previous studies reported the positive impact of TA on the viability and proliferation of fibroblast cells due to the interaction with imidazoles or thiols on the cytomembrane of fibroblast through its catechol groups via hydrogen bonding and hydrophobic interaction(Chang, Liu, Wang, Peng, & Ren, 2021) (He et al., 2020; Meng et al., 2021). Besides, TA can inhibit transforming growth factor-beta 1 (TGF-β1), resulting in the proliferation, migration, and gene expression involved in ECM remodeling in fibroblasts (Pattarayan, Sivanantham, Bethunaickan, Palanichamy, & Rajasekaran, 2018).

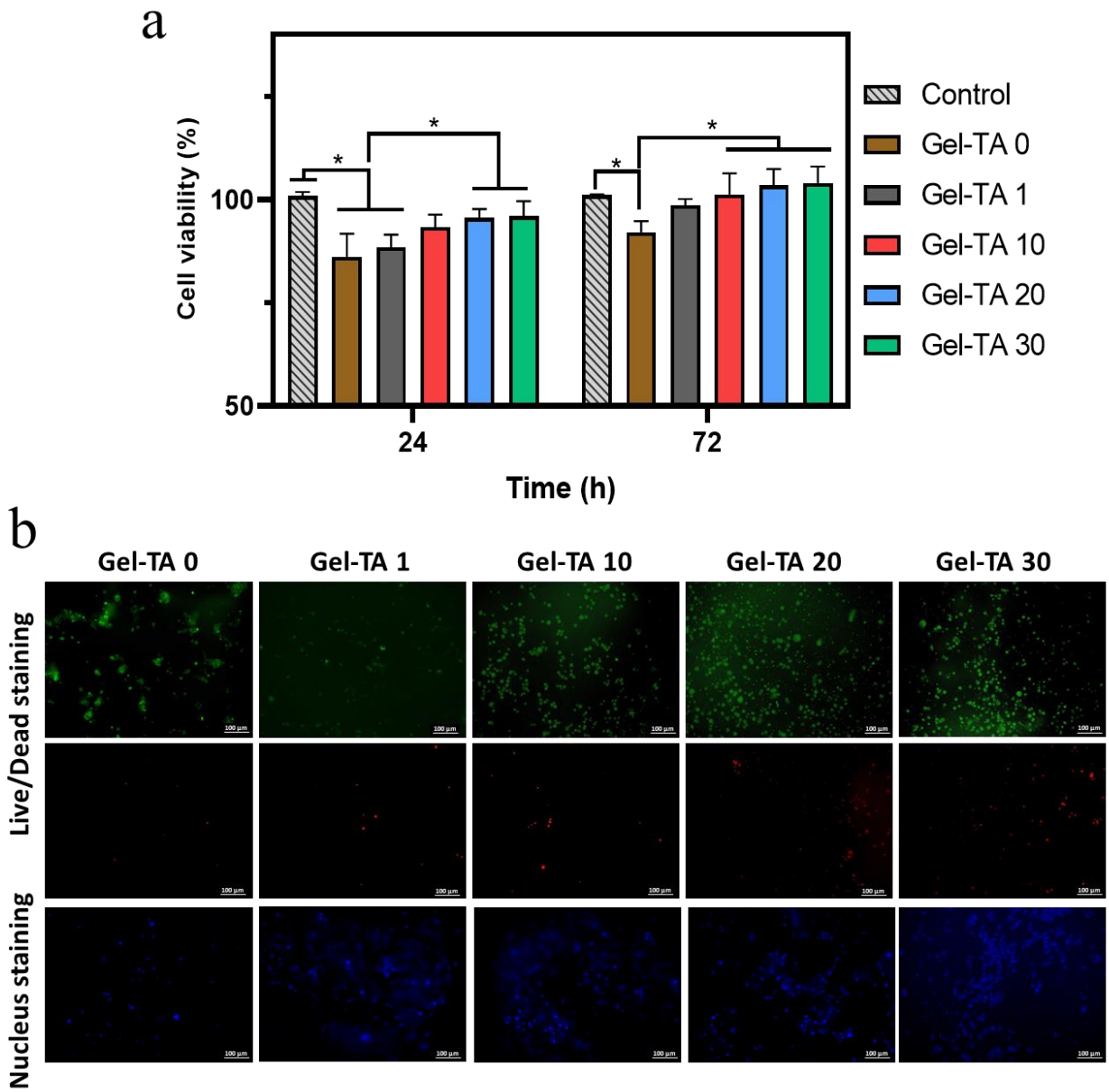

514

515 **Figure 7**. a) 3T3-L1 cell viability assessed by MTS assay after 24 and 72 h. Results are expressed as % cell
516 viability and are the mean ± SD of three independent experiments. Data were analyzed using a one-way
517 ANOVA test. *$p < 0.05$ as a compared type of hydrogel within each timepoint; b) Cell proliferation and
518 viability of 3T3-L1 fibroblast seeded on the Gel-TA hydrogels determined by live/dead staining and nucleus
519 staining using Hoechst 33258, scale bar: 100 µm.

520 Furthermore, a fluorescence staining of cell nuclei with Hoechst 33258 was used to track cellular
521 distribution seeded on the hydrogels (Fig 7a). The results showed that the Gel-TA 10, 20, and 30
522 hydrogels exhibited a uniform distribution of 3T3-L1 cells without aggregation, indicating the

hydrogels' capability to proliferate fibroblast cells. Increasing the TA concentration led to increased cell adherence on the hydrogel surface due to higher surface hydrophilicity and the presence of phenolic hydroxylic groups in TA, which can increase protein absorption further, resulting in better performance cell growth and proliferation (Xinyu Hu et al., 2017; Lv, Wang, Fu, Li, & Yu, 2020).

4. Conclusion

In summary, bioadhesive hydrogels were prepared by a facile soaking method of enzymatically crosslinked chitosan and alginate hydrogel in a tannic acid solution. The hydrogen bonding between TA and the chitosan and alginate chains strengthens the enzyme-mediated crosslinked hydrogel. The reinforcement showed a pH and TA concentration dependency and by increasing pH up to 7.4, significantly enhanced the crosslinking density due to the ionization of phenolic hydroxy groups on TA and subsequently formation of ionic interaction with the cationic chitosan. Besides, increasing TA concentration prolonged the degradation rate of the hydrogel by decreasing the swelling ratio and smaller pore size. The TA reinforcement improved both storage and loss moduli with the transition from frequency independent to frequency-dependent viscoelastic behavior, indicating the formation of non-covalent interaction. The hydrogel adhesiveness, antioxidant, antibacterial properties, as well as hydrogel cytocompatibility, and cell proliferation capability were significantly improved after the TA treatment. The Gel-TA hydrogel, with high mechanical stability, adhesiveness, and biological features, can be a promising candidate for biomedical application, particularly in wound healing.

Declaration of Competing Interest

The authors declare no conflict of interest.

Acknowledgments

H.J and A.S. acknowledge funding from Innoviris Brussels, Belgium (https://innoviris.brussels) under the project 2019 – BRIDGE – 4: RE4BRU. D.P. acknowledges the support from the Polish National Science Centre (2016/23/D/ST8/01267) and from the Academia Iuvenum, Wrocław University of Science and Technology. The content is solely the responsibility of the authors and does not necessarily represent the official views of the above-mentioned funding agency. The authors would

like to thank Dr. Véronique Fontaine and Dr. Christine Delporte for their assistance with the antibacterial and cell viability analysis and Dr. Bernaerts for assistance with the lap shear test experiment.

Data availability

The raw/processed data required to reproduce these findings cannot be shared at this time as the data also forms part of an ongoing study.

Reference

Abouelmagd, S. A., Abd Ellah, N. H., Amen, O., Abdelmoez, A., & Mohamed, N. G. (2019). Self-assembled tannic acid complexes for pH-responsive delivery of antibiotics: Role of drug-carrier interactions. *International Journal of Pharmaceutics,* 562, 76-85.

Ahmadian, Z., Correia, A., Hasany, M., Figueiredo, P., Dobakhti, F., Eskandari, M. R., . . . Hirvonen, J. (2021). A Hydrogen‐Bonded Extracellular Matrix‐Mimicking Bactericidal Hydrogel with Radical Scavenging and Hemostatic Function for pH‐Responsive Wound Healing Acceleration. *Advanced healthcare materials,* 10(3), 2001122.

An, X., Kang, Y., & Li, G. (2019). The interaction between chitosan and tannic acid calculated based on the density functional theory. *Chemical Physics,* 520, 100-107.

Bai, Z., Wang, T., Zheng, X., Huang, Y., Chen, Y., & Dan, W. (2021). High strength and bioactivity polyvinyl alcohol/collagen composite hydrogel with tannic acid as cross‐linker. *Polymer Engineering & Science,* 61(1), 278-287.

Bal-Ozturk, A., Cecen, B., Avci-Adali, M., Topkaya, S. N., Alarcin, E., Yasayan, G., . . . Avci, H. (2021). Tissue adhesives: From research to clinical translation. *Nano Today,* 36, 101049.

Bilotto, P., Labate, C., De Santo, M. P., Deepankumar, K., Miserez, A., & Zappone, B. (2019). Adhesive properties of adsorbed layers of two recombinant mussel foot proteins with different levels of DOPA and tyrosine. *Langmuir,* 35(48), 15481-15490.

Božič, M., Gorgieva, S., & Kokol, V. (2012). Homogeneous and heterogeneous methods for laccase-mediated functionalization of chitosan by tannic acid and quercetin. *Carbohydrate polymers,* 89(3), 854-864.

Cerdá, D. G., Ballester, A. M., Aliena-Valero, A., Carabén-Redaño, A., & Lloris, J. M. (2015). Use of cyanoacrylate adhesives in general surgery. *Surgery today,* 45(8), 939-956.

Chan, H.-M., Erathodiyil, N., Wu, H., Lu, H., Zheng, Y., & Ying, J. Y. (2020). Calcium cross-linked zwitterionic hydrogels as antifouling materials. *Materials Today Communications,* 23, 100950.

Chang, M., Liu, X., Wang, X., Peng, F., & Ren, J. (2021). Mussel-inspired adhesive hydrogels based on biomass-derived xylan and tannic acid cross-linked with acrylic acid with antioxidant and antibacterial properties. *Journal of Materials Science,* 56(26), 14729-14740.

Chen, C., Yang, X., Li, S.-j., Zhang, C., Ma, Y.-n., Ma, Y.-x., . . . Huang, X.-j. (2021). Tannic acid–thioctic acid hydrogel: a novel injectable supramolecular adhesive gel for wound healing. *Green Chemistry,* 23(4), 1794-1804.

Chen, K., Lin, Q., Wang, L., Zhuang, Z., Zhang, Y., Huang, D., & Wang, H. (2021). An All-in-One Tannic Acid-Containing Hydrogel Adhesive with High Toughness, Notch Insensitivity, Self-Healability, Tailorable Topography, and Strong, Instant, and On-Demand Underwater Adhesion. *ACS Applied Materials & Interfaces,* 13(8), 9748-9761.

Chen, Z., Wu, H., Wang, H., Zaldivar-Silva, D., Agüero, L., Liu, Y., . . . Zhao, J. (2021). An injectable anti-microbial and adhesive hydrogel for the effective noncompressible visceral hemostasis and wound repair. *Materials Science and Engineering: C,* 129(1), 112422.

Fan, H., Wang, J., & Jin, Z. (2018). Tough, swelling-resistant, self-healing, and adhesive dual-cross-linked hydrogels based on polymer–tannic acid multiple hydrogen bonds. *Macromolecules,* 51(5), 1696-1705.

Fan, H., Wang, J., Zhang, Q., & Jin, Z. (2017). Tannic acid-based multifunctional hydrogels with facile adjustable adhesion and cohesion contributed by polyphenol supramolecular chemistry. *ACS omega,* 2(10), 6668-6676.

García Cerdá, D., Ballester, A. M., Aliena-Valero, A., Carabén-Redaño, A., & Lloris, J. M. (2015). Use of cyanoacrylate adhesives in general surgery. *Surgery today,* 45(8), 939-956.

Ge, W., Cao, S., Shen, F., Wang, Y., Ren, J., & Wang, X. (2019). Rapid self-healing, stretchable, moldable, antioxidant and antibacterial tannic acid-cellulose nanofibril composite hydrogels. *Carbohydrate polymers,* 224, 115147.

Gülçin, İ., Huyut, Z., Elmastaş, M., & Aboul-Enein, H. Y. (2010). Radical scavenging and antioxidant activity of tannic acid. *Arabian journal of chemistry,* 3(1), 43-53.

Guo, J., Suma, T., Richardson, J. J., & Ejima, H. (2019). Modular assembly of biomaterials using polyphenols as building blocks. *ACS Biomaterials Science & Engineering,* 5(11), 5578-5596.

Guo, J., Suma, T., Richardson, J. J., Ejima, H. J. A. B. S., & Engineering. (2019). Modular assembly of biomaterials using polyphenols as building blocks. 5(11), 5578-5596.

Guo, J., Sun, W., Kim, J. P., Lu, X., Li, Q., Lin, M., . . . Qian, G. (2018). Development of tannin-inspired antimicrobial bioadhesives. *Acta biomaterialia,* 72, 35-44.

Gwak, M. A., Hong, B. M., & Park, W. H. (2021). Hyaluronic acid/tannic acid hydrogel sunscreen with excellent anti-UV, antioxidant, and cooling effects. *International journal of biological macromolecules,* 191, 918-924.

Han, L., Yan, L., Wang, K., Fang, L., Zhang, H., Tang, Y., . . . Weng, J. (2017). Tough, self-healable and tissue-adhesive hydrogel with tunable multifunctionality. *NPG Asia Materials,* 9(4), e372-e372.

Hao, S., Shao, C., Meng, L., Cui, C., Xu, F., & Yang, J. (2020). Tannic Acid–Silver Dual Catalysis Induced Rapid Polymerization of Conductive Hydrogel Sensors with Excellent Stretchability, Self-Adhesion, and Strain-Sensitivity Properties. *ACS Applied Materials & Interfaces,* 12(50), 56509-56521.

Haque, M. A., Kurokawa, T., & Gong, J. P. (2012). Super tough double network hydrogels and their application as biomaterials. *Polymer,* 53(9), 1805-1822.

He, X., Liu, X., Yang, J., Du, H., Chai, N., Sha, Z., . . . He, C. (2020). Tannic acid-reinforced methacrylated chitosan/methacrylated silk fibroin hydrogels with multifunctionality for accelerating wound healing. *Carbohydrate polymers,* 247, 116689.

Ho, Y.-C., Mi, F.-L., Sung, H.-W., & Kuo, P.-L. (2009). Heparin-functionalized chitosan–alginate scaffolds for controlled release of growth factor. *International journal of pharmaceutics,* 376(1-2), 69-75.

Hossain, K. M. Z., Calabrese, V., da Silva, M. A., Bryant, S. J., Schmitt, J., Scott, J. L., & Edler, K. J. (2020). Cationic surfactants as a non-covalent linker for oxidised cellulose nanofibrils and starch-based hydrogels. *Carbohydrate polymers,* 233, 115816.

Hu, X., Wang, Y., Zhang, L., & Xu, M. (2017). Morphological and mechanical properties of tannic acid/PAAm semi-IPN hydrogels for cell adhesion. *Polymer testing,* 61, 314-323.

Hu, X., Xia, X.-X., Huang, S.-C., & Qian, Z.-G. (2019). Development of adhesive and conductive resilin-based hydrogels for wearable sensors. *Biomacromolecules,* 20(9), 3283-3293.

I Erel-Unal, I., & Sukhishvili, S. A. (2008). Hydrogen-bonded multilayers of a neutral polymer and a polyphenol. *Macromolecules,* 41(11), 3962-3970.

Jafari, H., Dadashzadeh, A., Moghassemi, S., Zahedi, P., Amorim, C. A., & Shavandi, A. (2021). Ovarian Cell Encapsulation in an Enzymatically Crosslinked Silk-Based Hydrogel with Tunable Mechanical Properties. *Gels,* 7(3), 138.

Jafari, H., Delporte, C., Bernaerts, K. V., Alimoradi, H., Nie, L., Podstawczyk, D. A., . . . Shavandi, A. (2022). Synergistically complexation of phenol functionalized polymer induced in-situ microfiber formation for 3D printing of marine-based hydrogel. *Green Chemistry,* 24(6), 2409-2422.

Jafari, H., Delporte, C., Bernaerts, K. V., De Leener, G., Luhmer, M., Nie, L., & Shavandi, A. (2021). Development of marine oligosaccharides for potential wound healing biomaterials engineering. *Chemical Engineering Journal Advances,* 7, 100113.

Jing, X., Li, H., Mi, H.-Y., Liu, Y.-J., Feng, P.-Y., Tan, Y.-M., & Turng, L.-S. (2019). Highly transparent, stretchable, and rapid self-healing polyvinyl alcohol/cellulose nanofibril hydrogel sensors for sensitive pressure sensing and human motion detection. *Sensors and Actuators B: Chemical,* 295, 159-167.

Kaczmarek-Szczepańska, B., Mazur, O., Michalska-Sionkowska, M., Łukowicz, K., & Osyczka, A. M. (2021). The preparation and characterization of chitosan-based hydrogels cross-linked by glyoxal. *Materials,* 14(9), 2449.

Kaczmarek, B. (2020). Tannic acid with antiviral and antibacterial activity as a promising component of biomaterials—A minireview. *Materials,* 13(14), 3224.

Khanmohammadi, M., Dastjerdi, M. B., Ai, A., Ahmadi, A., Godarzi, A., Rahimi, A., & Ai, J. (2018). Horseradish peroxidase-catalyzed hydrogelation for biomedical applications. *Biomaterials science,* 6(6), 1286-1298.

Kim, E., Kim, M. H., Song, J. H., Kang, C., & Park, W. H. (2020). Dual crosslinked alginate hydrogels by riboflavin as photoinitiator. *International journal of biological macromolecules,* 154, 989-998.

Kumar, A., Nune, K., & Misra, R. (2018). Design and biological functionality of a novel hybrid Ti-6 A l-4 V/hydrogel system for reconstruction of bone defects. *Journal of tissue engineering and regenerative medicine,* 12(4), 1133-1144.

Le Thi, P., Lee, Y., Tran, D. L., Thi, T. T. H., Kang, J. I., Park, K. M., & Park, K. D. (2020). In situ forming and reactive oxygen species-scavenging gelatin hydrogels for enhancing wound healing efficacy. *Acta biomaterialia,* 103, 142-152.

Le, T. M. D., Duong, H. T. T., Thambi, T., Giang Phan, V., Jeong, J. H., & Lee, D. S. (2018). Bioinspired pH-and temperature-responsive injectable adhesive hydrogels with polyplexes promotes skin wound healing. *Biomacromolecules,* 19(8), 3536-3548.

Lee, H.-Y., Hwang, C.-H., Kim, H.-E., & Jeong, S.-H. (2018). Enhancement of bio-stability and mechanical properties of hyaluronic acid hydrogels by tannic acid treatment. *Carbohydrate polymers,* 186, 290-298.

Li, T., Song, X., Weng, C., Wang, X., Gu, L., Gong, X., . . . Chen, C. (2019). Silk fibroin/carboxymethyl chitosan hydrogel with tunable biomechanical properties has application potential as cartilage scaffold. *International journal of biological macromolecules,* 137, 382-391.

Li, X., Peng, X., Li, R., Zhang, Y., Liu, Z., Huang, Y., . . . Li, H. (2020). Multiple Hydrogen Bonds–Reinforced Hydrogels with High Strength, Shape Memory, and Adsorption Anti-Inflammatory Molecules. *Macromolecular rapid communications,* 41(14), 2000202.

Liang, H., Zhou, B., Wu, D., Li, J., & Li, B. (2019). Supramolecular design and applications of polyphenol-based architecture: A review. *Advances in colloid and interface science,* 272, 102019.

Liu, S., Liu, X., Ren, Y., Wang, P., Pu, Y., Yang, R., . . . Maurizot, V. (2020). Mussel-inspired dual-cross-linking hyaluronic acid/ε-polylysine hydrogel with self-healing and antibacterial properties for wound healing. *ACS Applied Materials & Interfaces,* 12(25), 27876-27888.

689 Lungu, R., Anisiei, A., Rosca, I., Sandu, A.-I., Ailincai, D., & Marin, L. (2021). Double functionalization
690 of chitosan based nanofibers towards biomaterials for wound healing. *Reactive and*
691 *Functional Polymers,* 167, 105028.
692 Lv, X., Wang, L., Fu, J., Li, Y., & Yu, L. (2020). A one-step tannic acid coating to improve cell adhesion
693 and proliferation on polydimethylsiloxane. *New Journal of Chemistry,* 44(35), 15140-15147.
694 McGill, M., Coburn, J. M., Partlow, B. P., Mu, X., & Kaplan, D. L. (2017). Molecular and macro-scale
695 analysis of enzyme-crosslinked silk hydrogels for rational biomaterial design. *Acta*
696 *biomaterialia,* 63, 76-84.
697 Meng, Z., He, Y., Wang, F., Hang, R., Zhang, X., Huang, X., & Yao, X. (2021). Enhancement of
698 Antibacterial and Mechanical Properties of Photocurable ε-Poly-l-lysine Hydrogels by Tannic
699 Acid Treatment. *ACS Applied Bio Materials,* 4(3), 2713-2722.
700 Moshayedi, S., Sarpoolaky, H., & Khavandi, A. (2021). Fabrication, swelling behavior, and water
701 absorption kinetics of genipin‐crosslinked gelatin–chitosan hydrogels. *Polymer Engineering*
702 *& Science,* 61(12), 3094-3103.
703 Nam, H. G., Nam, M. G., Yoo, P. J., & Kim, J.-H. (2019). Hydrogen bonding-based strongly adhesive
704 coacervate hydrogels synthesized using poly (N-vinylpyrrolidone) and tannic acid. *Soft*
705 *Matter,* 15(4), 785-791.
706 Nam, S., & Mooney, D. (2021). Polymeric tissue adhesives. *Chemical Reviews,* 121(18), 11336-11384.
707 Narasimhan, B. N., Deijs, G. S., Manuguri, S., Ting, M. S. H., Williams, M., & Malmström, J. (2021). A
708 comparative study of tough hydrogen bonding dissipating hydrogels made with different
709 network structures. *Nanoscale Advances,* 3(10), 2934-2947.
710 Pandey, A., & Negi, P. S. (2018). Phytochemical composition, in vitro antioxidant activity and
711 antibacterial mechanisms of Neolamarckia cadamba fruits extracts. *Natural product*
712 *research,* 32(10), 1189-1192.
713 Pattarayan, D., Sivanantham, A., Bethunaickan, R., Palanichamy, R., & Rajasekaran, S. (2018). Tannic
714 acid modulates fibroblast proliferation and differentiation in response to pro‐fibrotic
715 stimuli. *Journal of cellular biochemistry,* 119(8), 6732-6742.
716 Rezaei, N., Hamidabadi, H. G., Khosravimelal, S., Zahiri, M., Ahovan, Z. A., Bojnordi, M. N., . . . Darabi,
717 S. (2020). Antimicrobial peptides-loaded smart chitosan hydrogel: Release behavior and
718 antibacterial potential against antibiotic resistant clinical isolates. *International journal of*
719 *biological macromolecules,* 164, 855-862.
720 Rivero, R. E., Capella, V., Liaudat, A. C., Bosch, P., Barbero, C. A., Rodríguez, N., & Rivarola, C. R.
721 (2020). Mechanical and physicochemical behavior of a 3D hydrogel scaffold during cell
722 growth and proliferation. *RSC Advances,* 10(10), 5827-5837.
723 Ross‐murphy, s. b. (1995). Rheological characterisation of gels 1. *Journal of texture studies,* 26(4),
724 391-400.
725 Sakai, S., Kamei, H., Mori, T., Hotta, T., Ohi, H., Nakahata, M., & Taya, M. (2018). Visible light-induced
726 hydrogelation of an alginate derivative and application to stereolithographic bioprinting
727 using a visible light projector and acid red. *Biomacromolecules,* 19(2), 672-679.
728 Sakai, S., & Nakahata, M. (2017). Horseradish peroxidase catalyzed hydrogelation for biomedical,
729 biopharmaceutical, and biofabrication applications. *Chemistry–An Asian Journal,* 12(24),
730 3098-3109.
731 Schultz, W. (2007). Multiple dopamine functions at different time courses. *Annu. Rev. Neurosci.,* 30,
732 259-288.
733 Shutava, T., Prouty, M., Kommireddy, D., & Lvov, Y. (2005). pH responsive decomposable layer-by-
734 layer nanofilms and capsules on the basis of tannic acid. *Macromolecules,* 38(7), 2850-2858.
735 Shutava, T. G., & Lvov, Y. M. (2006). Nano-engineered microcapsules of tannic acid and chitosan for
736 protein encapsulation. *Journal of nanoscience and nanotechnology,* 6(6), 1655-1661.
737 Su, J., Sun, Y., Li, Z., Chen, Y., Ding, B., & Sun, W. (2019). Effect of tannic acid on lysozyme activity
738 through intermolecular noncovalent binding. *Journal of Agriculture and Food Research,* 1,
739 100004.

Sun, C., Xiong, B., Pan, Y., & Cui, H. (2017). Adsorption removal of tannic acid from aqueous solution by polyaniline: Analysis of operating parameters and mechanism. *Journal of colloid and interface science,* 487, 175-181.

Suneetha, M., Rao, K. M., & Han, S. S. (2019). Mussel-inspired cell/tissue-adhesive, hemostatic hydrogels for tissue engineering applications. *ACS omega,* 4(7), 12647-12656.

Taheri, P., Jahanmardi, R., Koosha, M., & Abdi, S. (2020). Physical, mechanical and wound healing properties of chitosan/gelatin blend films containing tannic acid and/or bacterial nanocellulose. *International journal of biological macromolecules,* 154, 421-432.

Thi, T. T. H., Lee, Y., Le Thi, P., & Park, K. D. (2019). Engineered horseradish peroxidase-catalyzed hydrogels with high tissue adhesiveness for biomedical applications. *Journal of Industrial and Engineering Chemistry,* 78, 34-52.

Tran, D. L., Le Thi, P., Thi, T. T. H., & Park, K. D. (2020). Novel enzymatically crosslinked chitosan hydrogels with free-radical-scavenging property and promoted cellular behaviors under hyperglycemia. *Progress in Natural Science: Materials International,* 30(5), 661-668.

Wang, F., Shi, W., Li, H., Wang, H., Sun, D., Zhao, L., . . . Xie, L. (2020). Decellularized porcine cornea-derived hydrogels for the regeneration of epithelium and stroma in focal corneal defects. *The Ocular Surface,* 18(4), 748-760.

Wang, R., Wang, X., Zhan, Y., Xu, Z., Xu, Z., Feng, X., . . . Xu, H. (2019). A dual network hydrogel sunscreen based on poly-γ-glutamic acid/tannic acid demonstrates excellent anti-UV, self-recovery, and skin-integration capacities. *ACS Applied Materials & Interfaces,* 11(41), 37502-37512.

Wen, J., Zhang, X., Pan, M., Yuan, J., Jia, Z., & Zhu, L. (2020). A robust, tough and multifunctional polyurethane/tannic acid hydrogel fabricated by physical-chemical dual crosslinking. *Polymers,* 12(1), 239.

Xie, D., Guo, J., Mehdizadeh, M. R., Tran, R. T., Chen, R., Sun, D., . . . Yang, J. (2015). Development of injectable citrate-based bioadhesive bone implants. *Journal of Materials Chemistry B,* 3(3), 387-398.

Yang, J., Li, M., Wang, Y., Wu, H., Zhen, T., Xiong, L., & Sun, Q. (2019). Double cross-linked chitosan composite films developed with oxidized tannic acid and ferric ions exhibit high strength and excellent water resistance. *Biomacromolecules,* 20(2), 801-812.

Zhan, F., Yan, X., Sheng, F., & Li, B. (2020). Facile in situ synthesis of silver nanoparticles on tannic acid/zein electrospun membranes and their antibacterial, catalytic and antioxidant activities. *Food Chemistry,* 330, 127172.

Zhang, W., Ling, C., Liu, H., Zhang, A., Mao, L., Wang, J., . . . Chen, J. (2020). Tannic acid-mediated dual peptide-functionalized scaffolds to direct stem cell behavior and osteochondral regeneration. *Chemical Engineering Journal,* 396, 125232.

Zhang, Z.-Y., Sun, Y., Zheng, Y.-D., He, W., Yang, Y.-Y., Xie, Y.-J., . . . Qiao, K. (2020). A biocompatible bacterial cellulose/tannic acid composite with antibacterial and anti-biofilm activities for biomedical applications. *Materials Science and Engineering: C,* 106, 110249.

Zhou, L., Fan, L., Yi, X., Zhou, Z., Liu, C., Fu, R., . . . Yu, P. (2018). Soft conducting polymer hydrogels cross-linked and doped by tannic acid for spinal cord injury repair. *ACS nano,* 12(11), 10957-10967.